WELDING RESEARCH

SUPPLEMENT TO THE *WELDING JOURNAL*, December 2002
Sponsored by the American Welding Society and the Welding Research Council

Determination of Gradients in Mechanical Properties of 2.25Cr-1Mo Weldments Using Shear-Punch Tests

A test technique was developed to more accurately determine mechanical properties of individual regions in the HAZ

BY V. KARTHIK, K. V. KASIVISWANATHAN, K. LAHA, AND B. RAJ

ABSTRACT. The heat-affected zone (HAZ) of 2.25Cr-1Mo steel weldments consists of coarse-grained bainite, fine-grained bainite, and intercritical structures. Mechanical properties of the individual regions of the HAZ are difficult to determine by conventional methods because of the difficulty in making mechanical test pieces of adequate dimensions from the individual microstructures of very small regions in the HAZ. This paper describes the use of shear punch tests to determine the mechanical properties of the individual regions in the HAZ. A linear correlation established between the tensile properties and the corresponding properties obtained from the shear punch test of various heat-treated structures was used to characterize the mechanical properties for individual regions in the HAZ of actual weldments.

Introduction

The evaluation of gradients in mechanical properties that exist in a weldment is essential for understanding the behavior of welded structures employed in high-performance applications. The microstructures that evolve in a weldment (comprised of base metal, heat-affected zones (HAZ), and weld metal) are heterogeneous due to the temperature gradients associated with the welding process and the chemical gradients that evolve during the process. During welding, the peak temperatures attained and the subsequent cooling rates decrease with increasing distance from the fusion boundary, leading to the formation of various nonequilibrium microstructures across the heat-affected zone (HAZ). This microstructural inhomogeneity is most severe in dissimilar or multipass welds, resulting in gradients in mechanical properties across the individual zones of the weldments. It is practically impossible to obtain standard specimens cut from individual regions of the weldment for evaluating mechanical properties by conventional test techniques due to the narrowness of the various zones. Therefore, early investigators resorted to a variety of special heat-treatment techniques to obtain sizeable volumes of materials that would approximate the individual weld/HAZ microstructures (Ref. 1). However actual microstructures that evolve in a weldment with the formation of substructure and precipitation kinetics can never be fully simulated by these methods. Therefore, mechanical properties evaluated from specimens prepared by heat treatment techniques that simulate weld microstructures are not true representatives of weldments.

An attempt has been made for the first time to utilize a recently developed miniature test technique to get a more accurate estimation of the mechanical properties in various zones of weldments. The material chosen for the current study is low-alloy ferritic 2.25Cr-1Mo steel, which is used extensively as a structural material in steam generating systems of both nuclear and conventional power plants. In welded 2.25Cr-1Mo steel structures, a high percentage of failures have been reported in the HAZ of these weldments (Ref. 2). Hence, it is essential to understand the yield and fracture behavior of 2.25Cr-1Mo weldments by characterizing the mechanical property gradients in the HAZ. For a single weld bead on 2.25Cr-1Mo steel plate, typical microstructures obtained in the weld and HAZ are shown schematically in Fig. 1. It can be seen from Fig. 1 that the HAZ consists of three distinct zones, namely the prior austenitic coarse-grained bainite, the prior austenitic fine-grained bainite, and the intercritical (ICR) microstructures. It is well known that the bainitic microstructure is a two-phase structure of α-ferrite (BCC) and cementite (orthorhombic).

The three principal microstructures in the HAZ depend on the peak temperatures attained in the different regions during multipass welding. The regions closest to the fusion boundary experience peak temperatures above Ac_3. At these temperatures, the carbides dissolve and, hence, coarse-grained austenite develops, which transforms to a coarse-grained bainitic structure on cooling. With increasing distance from the weld interface, the peak temperature experienced by the HAZ decreases, resulting in a fine-grained bainitic structure. When the thermal cycle peak temperature seen by the HAZ is between Ac_1 and Ac_3, only partial transformation to austenite takes place during heating and a mixture of austenite-transformed products with ferrite (intercritical struc-

V. KARTHIK, K. V. KASIVISWANATHAN, K. LAHA, and B. RAJ are with the Metallurgy and Materials Group, Indira Gandhi Centre for Atomic Research, Kalpakkam, India.

KEY WORDS

Gradients
Heat-Affected Zone (HAZ)
Mechanical Properties
Microstructure
Miniature Tests
Punch Test

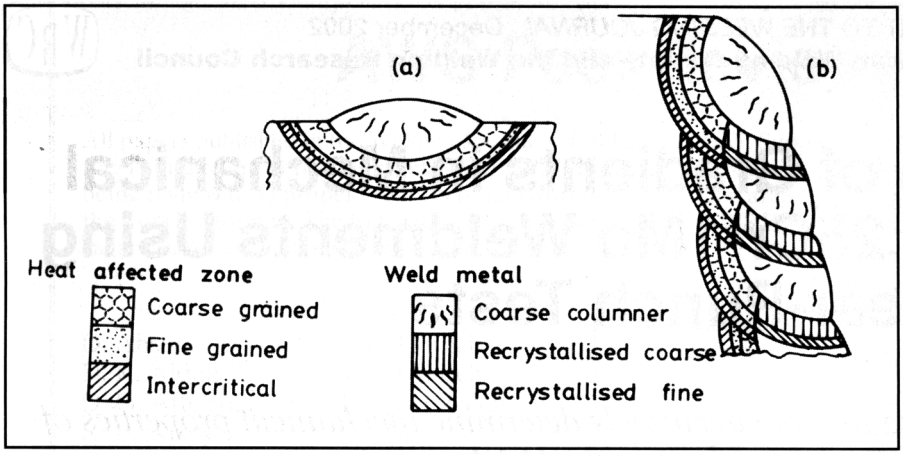

— *Schematic repr*
nultipass.

1Mo steel weldments *Single pas*

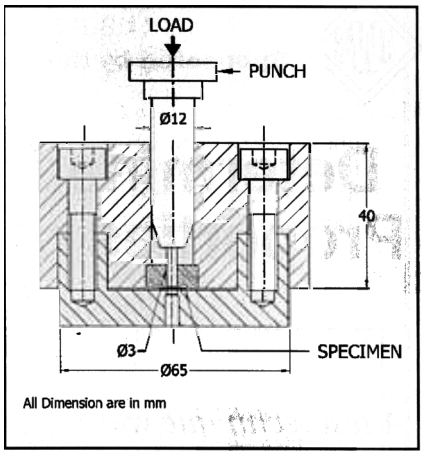

Cross section of shear punch fixture

Table 1 — Summary of Various Heat Treatments on 2.25Cr-1Mo Steel with the Resultant Microstructures and Hardness Values

Sampl ID	Temperature Kelvin	Details of He Time t Min	treatment Hardnes HVN	Resultant Microstructure
	B:	—	200	70% Bainitic- 30% Ferritic
	Weld metal			Lath bainite structure
	1083			Mixed ferrite and 13.44 austenite-transformed product
			.4	Mixed ferrite and 16.95 austenite-transformed product
				Mixed ferrite and 20% austenite-transformed product
	1128			Mixed ferrite and 33.44 austenite-transformed product
	1138			Mixed ferrite and 61.6% austenite-transformed product
				Mixed ferrite and 98 austenite-transforme product
				Mixed ferrite and 10 austenite-transforme product
10			96	100% fine-grained bainite 0% coarse-grained bainit

Heating to te
(a) Normaliz

lowed by
K for 60

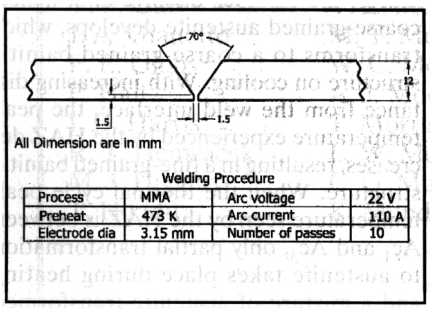

Fig. *Details of*

ture) is formed on cooling. The mechanical properties of these individual regions are difficult to obtain by conventional methods because of the difficulties in making mechanical test pieces of adequate dimensions with individual microstructures from very small regions in the HAZ.

The current work demonstrates the usefulness of a miniature-specimen test technique to determine the mechanical properties of the individual regions of HAZ of 2.25Cr-1Mo steel weldments. Miniature-specimen test techniques enable the characterization of mechanical behavior by using an extremely small volume of the material. These miniature-specimen test techniques can be broadly classified into the following categories:

1) Tests based on miniaturization or scaling down of conventional specimen size (similar to miniature tensile, fatigue, impact, and fracture toughness tests). The specimens used here are very small relative to their conventional counterparts.

2) Tests based on novel techniques using disk-sized specimens of approximately 0.3 mm thickness (like disk bend tests, shear/small punch tests).

3) In-situ mechanical test microprobes based on dynamic ball indentation techniques (Ref. 3).

This paper describes the use of the shear punch (ShP) test technique to determine strength and ductility parameters by using extremely thin specimens extracted from various regions of the HAZ. The ShP test utilizes a cylindrical punch with a flat end to punch a hole in a disk-sized specimen axisymmetrically. The load-displacement curve obtained from the ShP test is analyzed to extract the uniaxial tensile properties (Refs. 4–6). Since the test technique requires only a very small volume of test material, it can be applied to thin sections cut out from various regions of the HAZ. It has been found the yield and maximum loads in the shear punch can be correlated with the uniaxial tensile yield and ultimate strengths, respectively. Tensile uniform elongation can also be predicted from shear punch data. The correlation equations between tensile data and the corresponding ShP test data are basically empirical in nature. Hamilton et al. (Ref. 7) has experimentally shown these correlation equations vary with alloy class.

To obtain correlation between the uniaxial tensile properties and shear punch

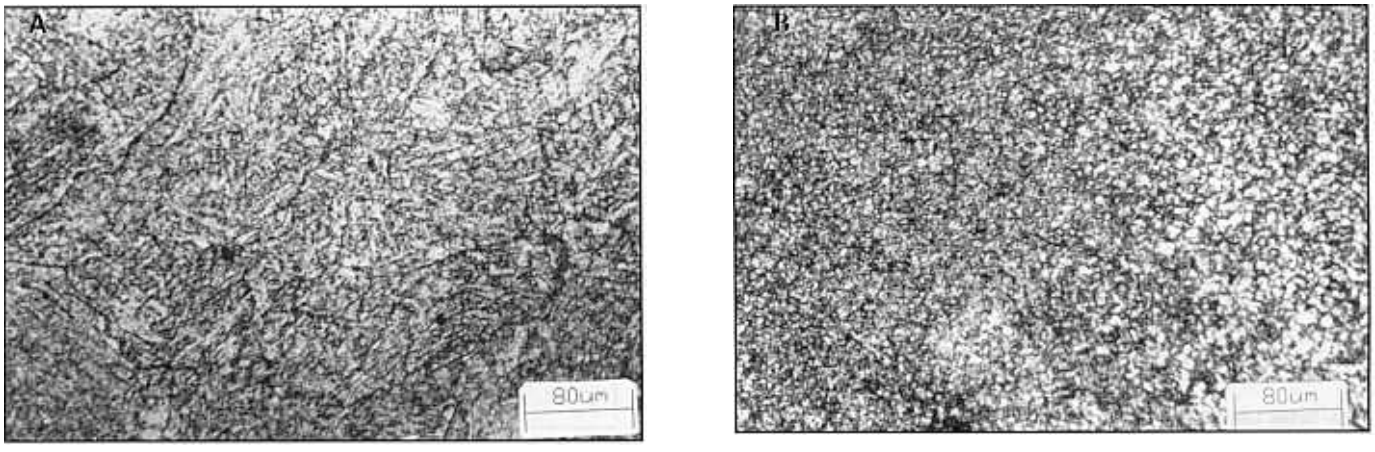

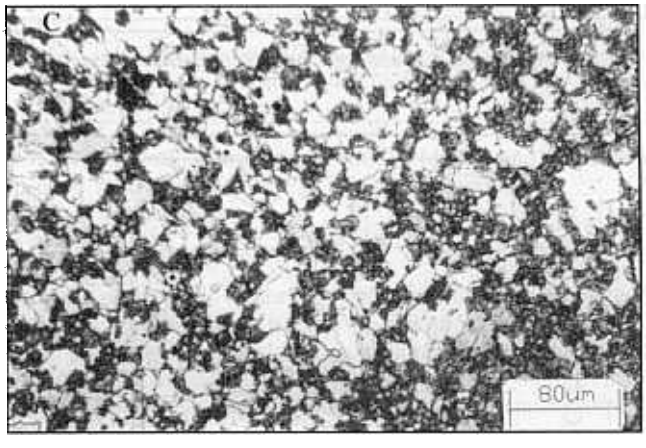

Fig. 4 — Microstructure of the ShP test specimens extracted from the individual HAZ regions of a 2.25Cr-Mo weld joint. A — Coarse-grain bainite; B — fine-grain bainite; C — intercritical region.

test data, specimens from various heat-treated 2.25Cr-1Mo steel with widely varying microstructures and tensile properties were used. ShP tests were carried out on specimens taken from the collar portion of the tensile test coupon with corresponding microstructure. A shear-tensile correlation established from an extensive database was then used to establish the mechanical properties of individual regions of the HAZ for a 2.25Cr-1Mo weldment.

Experimental Procedure

The 2.25Cr-1Mo steel base metal (normalized at 1223 K for 17 min and tempered at 1003 K for 60 min) was subjected to a variety of heat treatments to obtain widely varying microstructures and mechanical properties. This includes the simulation of microstructures, namely the coarse-grained bainite, the fine-grained bainite, and the intercritical (ICR) structures expected in the HAZ of a 2.25Cr-1Mo weldment. The parameters for heat treatments were selected to obtain the range of expected strength values in the HAZ and, thereby, ensure the validity and further improve the accuracy of the thus-arrived correlation. Table 1 summarizes the details of various heat treatments with the resultant microstructures and hardness values. The simulation treatments were carried out by 1) inserting rough machined base metal bars (60 x 12 x 12 mm) in a resistance heating furnace at 873 K, 2) heating for 30 to 40 min to attain peak temperatures in the range 1083–1473 K, 3) soaking for a selected time (1–5 min) followed by oil quenching, and 4) tempering at 973 K/1 h. Cylindrical tensile specimens (26-mm gauge length and 4-mm diameter) were fabricated from the different heat-treated microstructures. Tensile tests were carried out at a nominal strain rate of 3 x 10^{-4} s^{-1} at ambient temperature (298 K) using a floor model Instron 1195 Universal testing machine.

ShP test specimens were cut from the collar region of uniaxially tensile-tested specimens of different heat-treated structures mentioned above. The specimens were cut using a high-precision, slow-speed, thin-wafer tool, which resulted in a uniformly thick specimen that required only mechanical polishing with 600-grit SiC paper to achieve the required uniformity in thickness of ± 0.01 mm. Uniformity in specimen thickness (± 0.01 mm) was maintained to ensure good contact with the die surface. For carrying out the ShP test, a test fixture was developed at the authors' laboratory, shown schematically in Fig. 2. Shear-punch tests were performed at room temperature by forcing the flat cylindrical punch through the specimen clamped in the fixture using a desktop servo-hydraulic universal testing machine (BiSS make). The loading rate of all the shear punch tests carried out was maintained at 0.10 mm/min. The stress in a ShP test is primarily shear stress with contributions from compression, stretching, and bending in the deformation region between the punch and the die (Ref. 8). Unlike tensile tests, there are no means for measuring the strain in the specimen, and this can be only approximated by the punch displacement. Due to the characteristic loading configuration and the complex stress states in the specimen during the test, it may not be possible to quantify the nominal shear strain rate in a ShP test. Hence, the approximate strain rate determined from the ratio of punch speed to initial specimen thickness is 5 x 10^{-3}/s, while the nominal strain rate in a tensile test is 3 x 10^{-4}/s. However, it can be seen the crosshead speed is of the same order in both the tensile and shear punch tests (i.e., 0.1 mm/min). Load was monitored with a standard load cell (30 kN) in its reduced range of ± 3.75 kN (accuracy ± 1% of the range). A minimum of four shear punch tests were performed for each heat-treated microstructure.

To establish the mechanical properties of individual regions of the HAZ for 2.25 Cr-1 Mo weldments, plates of 12 mm thickness were welded together by shielded metal arc welding (SMAW)

Table 2 · Chemical Composition of the Base and Weld Metals

	Element (wt-%)							
Material	C	Si	Mn	P	S	Cr	Mo	Fe
Base	0.06	0.18	0.48	0.008	0.008	2.18	0.93	Balance
All weld	0.05	0.4	0.72	0.02	0.012	2.3	1.1	Balance

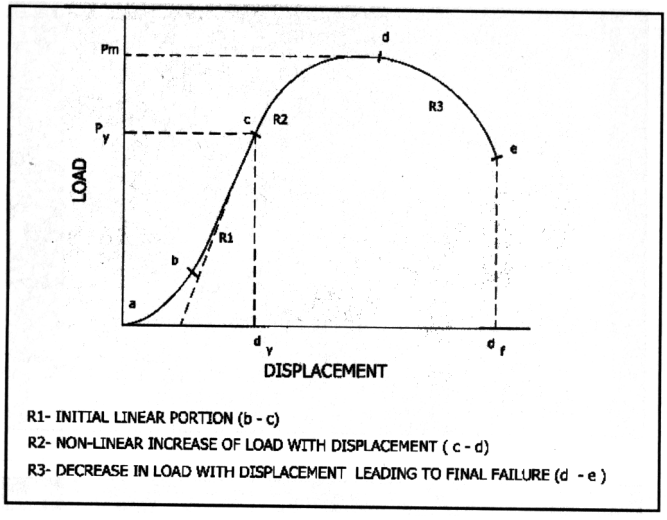

Fig. 5 Typical load-displacement curve obtained in a shear punch test.

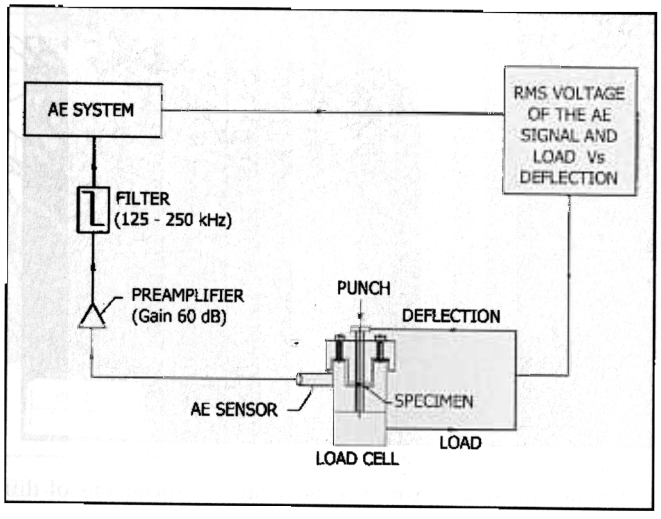

Fig. 6 — Diagram of shear punch experimental setup for on-line acoustic emission (AE) monitoring

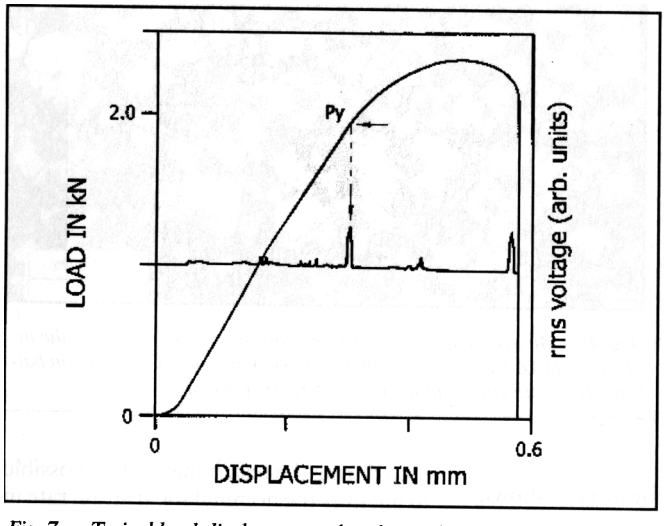

Fig. 7 — Typical load-displacement plot obtained during shear punch test with acoustic emission (AE) signal superimposed.

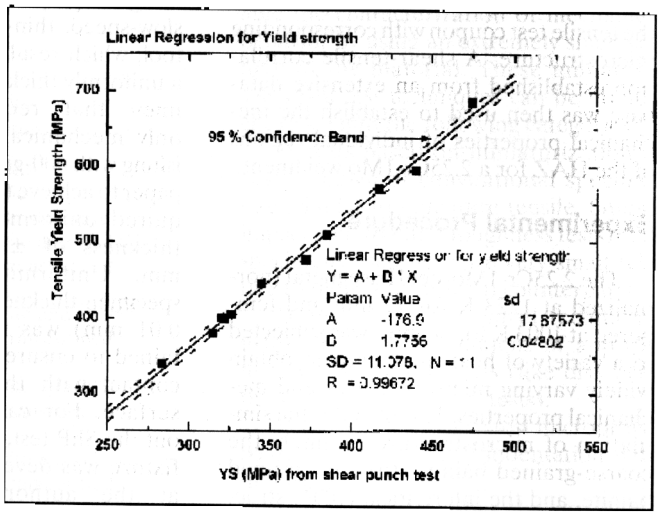

Fig. 8 — Average tensile yield vs. shear punch yield strength of various heat-treated microstructures (regression line and 95% confidence band are also shown).

using basic-coated 2.25Cr-1Mo electrodes. Details of the weld edge preparation are shown in Fig. 3. The chemical compositions of the weld and base metals are given in Table 2. The weld pads were examined by radiography for their soundness. Locating the region of HAZ by optical microscopy, specimens from coarse-grained bainite, fine-grained bainite, and intercritical regions in the HAZ were cut using an Isomet cutting machine (0.6-mm SiC tool). Metallographic examinations were carried out on both sides of the specimen by optical microscopy to ensure homogeneity of structure within a shear punch specimen. Figure 4 shows the microstructures of the shear punch test specimens extracted from the HAZ of the weldments. Shear punch tests were carried out on HAZ specimens with the setup mentioned above.

Results and Discussion

A typical load-displacement curve obtained from the ShP test is shown in Fig. 5. The curve is similar to the load-displacement plot of a conventional tensile test. The curve exhibits an initial linear portion (region 1), deviation from linearity (P_y), nonlinear increase of load with displacement (region 2), and decrease in load with displacement (region 3), leading to final failure. Details of data analysis of the ShP tests are discussed elsewhere (Refs. 4–7).

Shear Punch Tensile Strength Correlation

The tensile strength parameters, such as the 0.2% proof stress (YS) and ultimate tensile strength (UTS), were obtained from tensile test data of various microstructures of 2.25Cr-1Mo steel as given in Table 3.

In the ShP test, the ShP maximum stress is estimated from the maximum point P_m on the load-displacement curve, as shown in Fig. 5. The ShP yield stress is evaluated using the load corresponding to the point of deviation from linearity in the initial portion of the load-displacement curve corresponding to the points (d_y, P_y) of the load-displacement curve shown in Fig. 5.

The acoustic emission technique (AET) was used in the present study for a more accurate determination of the yield load in the ShP test. Acoustic emission (AE) occurs during deformation due to rapid release of transient energy from localized sources such as dislocation movements, phase transformation, crack formation, and extension. Studies of emission from ferritic steels under uni-

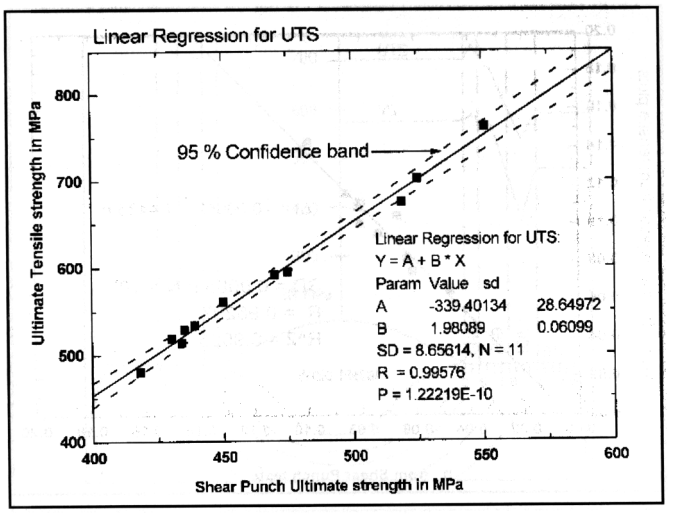

Fig. 9 — Average ultimate tensile strength vs. shear punch maximum strength of various heat-treated microstructures (regression line and the 95% confidence band are also shown).

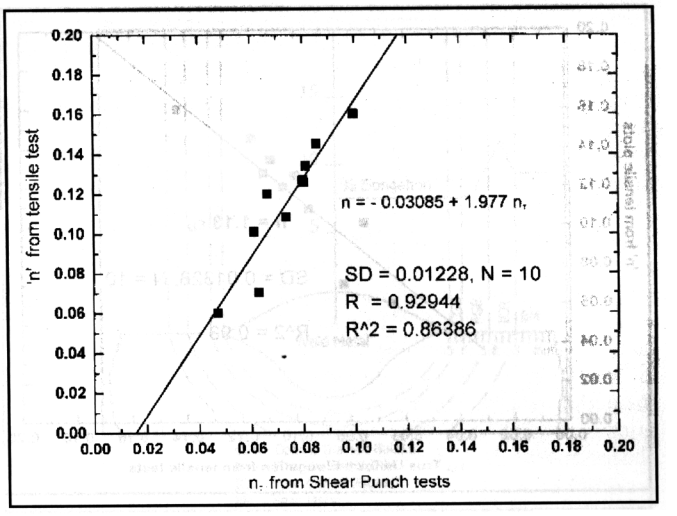

Fig. 10 — n calculated from log-log plots of σ vs. ε plotted against n_τ for various heat-treated microstructures of 2.25Cr-1Mo steel.

axial loading show pronounced AE activity occurs on the onset of yielding and has been associated with dislocation motion, dislocation multiplication, and Luders-band propagation (Ref. 9). Acoustic emission activity in such steels beyond the post yield region at different plastic strains has been attributed to carbide fracture and decohesion/fracture of inclusions (Ref. 10). Acoustic emission monitoring was used in ShP tests to locate the yield load for 2.25Cr-1Mo steel (Ref. 11). The peak in the root mean square (rms) voltage of the continuous AE signal was used to characterize yielding during ShP testing. A piezoelectric transducer having a resonant frequency of 175 kHz, preamplifier (60-dB gain) and a compatible filter (125–250 kHz) were used to capture the AE signal. The AE sensor was fixed on the test fixture close to the sitting plane of the specimen. The smooth machined surfaces of the die seat and specimen ensured good acoustic contact and signals to the transducer. High-vacuum grease was used as the acoustic couplant between the transducer and the die. A gain of 96 dB and a threshold of 1.15 V were selected so no external noise was picked up. The details of the AE monitoring setup used for this study are shown in Fig. 6. The curve showing the variation of the rms voltage for the AE signal with displacement is superimposed onto the load-displacement plots as shown in Fig. 7. It was found the continuous rms voltage indicated two prominent peaks, one corresponding to the yield load in region R_2 of the load-displacement curve and the other corresponding to failure of the specimen. The location of the peak rms voltage of the AE signal in region R_2 of the load-displacement curve is an indication of the yield point. It was found the yield point determined from AET closely correlated with that determined by the point of deviation from linearity (d_y, P_y) in the load-displacement curve for this class of alloy (Ref. 11).

The ShP test produces a state of stress that is not pure shear, and the shear punch strengths cannot be truly considered to be shear yield and shear maximum strengths. They are referred to as shear punch effective yield (τ_y) and effective maximum strength (τ_u), respectively (Ref. 7).

The shear punch strengths are determined for both yield (P_y) and maximum load (P_m) using the equation

$$\tau = P/(2\pi\, r\, t) \qquad (1)$$

where τ = shear punch effective yield (t_y) or effective maximum strength (t_u); P = yield load corresponding (P_y) and maximum load (P_m) for effective yield strength and effective maximum strength, respectively; t = initial specimen thickness; and r = punch radius.

Four ShP tests were carried out for each microstructural condition. The shear effective yield and maximum strengths obtained on four specimens with the same microstructure exhibited a maximum scatter of ~14 MPa and ~9 MPa, respectively. The average shear effective yield (τ_y) and effective maximum strengths (τ_u) obtained by ShP tests on various microstructures of 2.25Cr-1Mo steel are tabulated in Table 3. The shear punch test results of Table 3 are not to be directly compared with the corresponding tensile test results. A linear correlation is obtained between the tensile properties and corresponding shear punch test properties using the data in Table 3.

Table 3 — Data on Mechanical Properties Obtained from Tensile and Shear Punch Tests of Various Heat-Treated Microstructures of 2.25Cr-1Mo Steel

	Tensile Test Results					Shear Punch Test Results			
Sample ID	UTS σ_u MPa	YS σ_y MPa	ε_u%		% $RA_{tensile}$	τ_u MPa	τ_y MPa	n_τ	% $(RA)_{shp}$
1	591	476	10.43	0.12	81.2	470	372.2	0.066	76
2	702	595	—			525	440	—	
3	519	400	11.15	0.127	78.3	430	320	0.080	78
4	514	380	11.57	0.145	82.46	434	315	0.085	
5	480	339	14.29	0.16	83	418	283.29	0.099	82.4
6	529	399.2	10.88	0.134	75	435	322	0.081	82.9
7	534	405	10.01	0.126	79.2	439	326	0.080	82.6
8	561.2	444	9.495	0.108	79.9	450	345	0.073	76.6
9	594	508.6	7.481	0.101	83	475	385	0.061	77
10	674	570	8.25	0.07	81.5	519	417.5	0.063	80.9
11	762	685	6.48	0.06	65.3	551	474.25	0.047	60

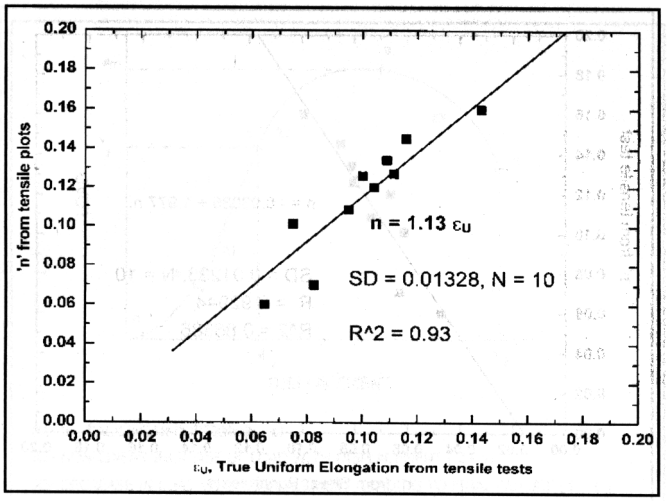

Fig. 11 — n determined from log-log plots of σ vs. ε plotted against ε_u determined from tensile test traces of various heat-treated structures of 2.25Cr-1Mo steel.

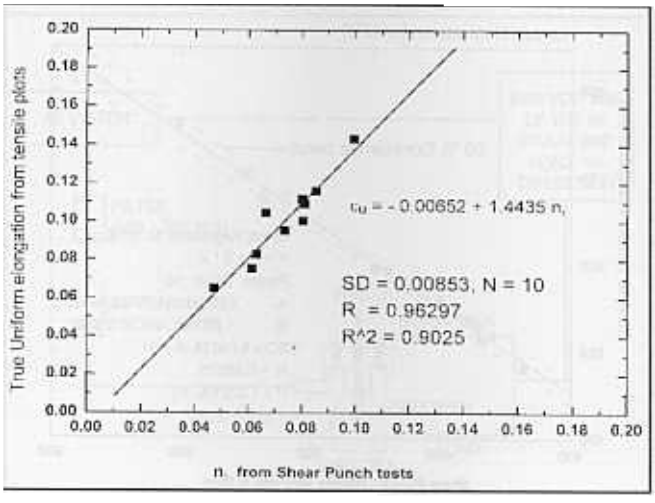

Fig. 12 — Plot of ε_u vs. n_τ for various heat-treated structures of 2.25Cr-1Mo.

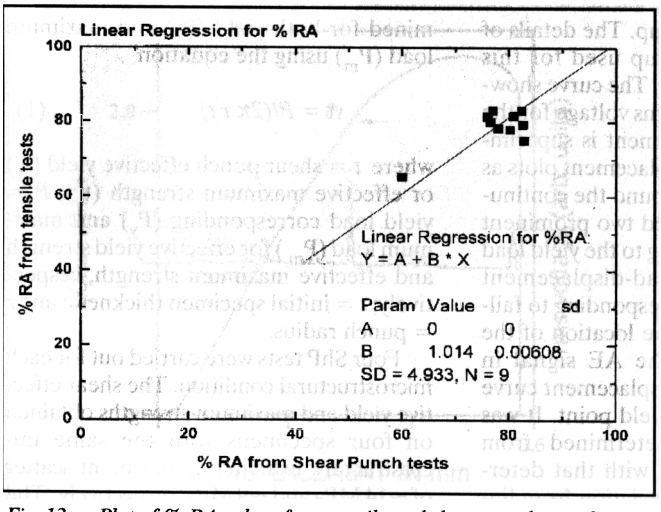

Fig. 13 — Plot of % RA values from tensile and shear punch tests for various heat-treated structures of 2.25Cr-1Mo steel.

The shear punch strength data ($\tau_{y,u}$) of the various microstructures plotted against their corresponding uniaxial tensile data ($\sigma_{y,u}$) are shown in Fig. 8 (YS vs. τ_y) and Fig. 9 (UTS vs. τ_u). When corresponding sets of τ and σ are plotted, they fall along a straight line. A least-squares linear regression is performed to obtain the constants A and B of the equation

$$\sigma_{y,u} = A + B\,t_{y,u} \qquad (2)$$

where σ is the uniaxial tensile stress and τ is the shear punch stress. The linear regression equations obtained for the yield load (Fig. 8) and maximum load (Fig. 9) conditions, respectively, are

$$\sigma_y = -176.92 + 1.78\,\tau_y \qquad (3A)$$

$$\sigma_u = -339.40 + 1.98\,\tau_u \qquad (3B)$$

where both τ and σ are in MPa with the regression coefficient (r) values of 0.99 for both regressions.

The effectiveness of the above correlation is inferred by estimating the standard deviation of the measured tensile property from the value that the correlation predicts from the shear punch data, which is 9 MPa for UTS-τ_u correlation and 11 MPa for YS-τ_y correlation. The reliability of the predicted tensile properties is established by constructing a 95% confidence band for the predicted value. The 95% confidence band on the predicted σ for a given τ is found to be ~± 2.5% of σ_y for YS and ~± 2% of σ_u for UTS, as shown in Figs. 8 and 9, respectively.

Earlier work summarized by Hamilton et al. (Ref. 7) showed there was a range of values observed for both A and B depending on the alloy class. The values of slope A were shown to range from 1.7 to 2.2 for yield and 2.0 to 2.6 for maximum stress. The constants obtained in the current study are consistent with that obtained for a similar alloy class in the recent studies (Ref. 7).

Shear Punch: Tensile Ductility Correlation

Tensile uniform elongation has also been predicted from ShP properties (Ref. 12). The mathematical definition of power law strain hardening (PLSH) is given by

$$\sigma = K\,(\varepsilon_{pl})^n \qquad (4)$$

where σ and ε_{pl} are the true stresses and strains, n is the tensile strain hardening exponent, and K is the strength coefficient (Ref. 13). From the above equation and the definition of necking, it can be derived that

$$n = \varepsilon_U \qquad (5)$$

where ε_U is the true uniform elongation obtained from tensile tests. The tensile test strain hardening exponent n is obtained from the slope of the log-log tensile test plots of σ vs. ε_{pl} using Equation 4, and the true uniform elongation ε_U is measured as the true plastic strain up to maximum load, from the tensile test plots.

It is required to determine the strain hardening exponent n_τ from the load-displacement data of ShP tests. The idea is to correlate n and ε_U obtained from tensile data with n_τ of ShP tests. But for a ShP test, it is not possible to readily convert load vs. displacement data to stress-strain values from which n_τ can be estimated. This is due to the complex stress states in the specimen during deformation in ShP tests. Hence, the following relationships have been used for a simple estimate of n_τ from ShP test data:

For a tensile test

$\sigma_u = K\,(n)^n$ corresponding to UTS and $\sigma_y = K\,(0.002)^n$ corresponding to 0.2% yield stress

Combining the above equations

$$(n/0.002)^n = (\sigma_u/\sigma_y) \qquad (6)$$

To determine the strain hardening exponent n_τ in a ShP test, (σ_u/σ_y) is replaced with (τ_u/τ_y) in the above equation, resulting in

$$(n_\tau/0.002)^n\tau = (\tau_u/\tau_y) \qquad (7)$$

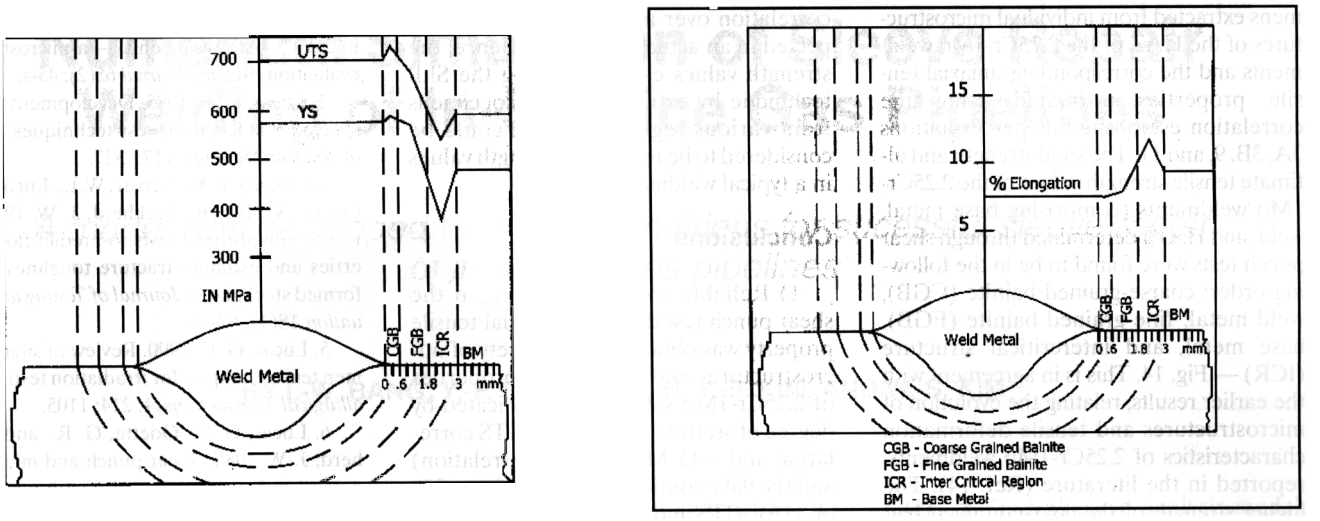

Fig. 14 — Mechanical property gradients across various regions of the HAZ of 2.25Cr-1Mo steel weldments estimated from shear punch tests.

where n_τ is the strain-hardening exponent determined using the τ_u and τ_y values obtained in a ShP test. It is seen that n from tensile tests and n_τ from ShP tests does not follow a 1:1 relationship, but can be linearly correlated. This shows that Equation 7 is only a semiempirical relationship to estimate n_τ. The values of n and ε_U obtained from tensile test data and n_τ from ShP test data for various simulated microstructures are tabulated in Table 3.

A linear relationship was found to exist between n (determined from the log-log plots of σ vs. ε_{pl}) and n_τ with an r^2 coefficient of 0.86 — Fig. 10. The n obtained from log-log tensile plots was compared with the true uniform elongation ε_U (also obtained from tensile plots) for all the microstructures. It is seen from Fig. 11 that $n = 1.1\ \varepsilon_U$ with $r^2 = 0.93$, for the different microstructures of 2.25Cr-1Mo steel. This implies the tensile flow behavior of all microstructural conditions of 2.25Cr-1Mo steel and its weldments can be adequately described by the Hollomon equation (Equation 4) and the resulting approximation $n \approx \varepsilon_U$.

An attempt was made to obtain a linear relationship between true elongation ε_U of the tensile data and n_τ obtained from ShP tests for the various microstructures. A least squares linear regression is performed to obtain the constants C and D of the equation.

$$\varepsilon_u = C + D\,n_\tau \qquad (8)$$

A linear relationship was found to exist between ε_U and n_τ (Fig. 12), and there appears to be less data scatter compared to the n vs. n_τ plot. This can be seen from the r^2 coefficient, which is 0.90 for ε_U vs. n_τ plot (Fig. 12) as compared to 0.86 for n vs. n_τ plot (Fig. 10), indicating a better correlation between ε_U vs. n_τ. The linear regression equation obtained for ε_U-n_τ correlation using the data in Table 3 is

$$\varepsilon_U = -0.00652 + 1.44357\,n_\tau \qquad (9)$$

An attempt was made to calculate the reduction in area (RA) based on displacement from yield point to failure using the equation

$$RA = (d_f - d_y)/t \qquad (10)$$

where d_f is displacement to failure in mm, d_y is displacement to yield in mm, and t is initial specimen thickness in mm.

Some difficulty was encountered in the measurement of d_f due to variations observed in the load-displacement curve beyond the maximum load in the four or five ShP tests carried out on specimens of the same microstructure. Hence, the % RA values reported here is an average of two tests, from each microstructure. The % RA calculated as per the above procedure for the ShP tests are compared with the % RA values obtained from the tensile tests as shown in Fig. 13. A reasonably good agreement was observed for the % RA values between the ShP test and the tensile test. The linear regression equation obtained for RA correlation is

$$\%(RA)_{tensile} = 1.013\%(RA)_{Shp}$$
standard deviation is 4.9%. (11)

Equations 3A, 3B, 9, and 11 are the correlation equations obtained between the tensile properties and corresponding shear punch test properties using the data in Table 3. The above results clearly show that shear punch test data can be reliably correlated to determine the uniaxial tensile properties (both strength and ductility) for a range of microstructures and mechanical properties for 2.25Cr-1Mo ferritic steels. The tensile-shear punch correlation is effectively independent of starting state condition over a very wide range of microstructures, whether they are induced thermally or by mechanical treatment. This clearly brings out the possibility of using the ShP test to estimate the property gradient (both strength and ductility) in an actual weldment using small specimens extracted from the various regions of the HAZ of a 2.25Cr-1Mo weldment.

Table 4 summarizes the data obtained from the shear punch testing of the speci-

Table 4 — Mechanical Properties of the Various Regions of HAZ Estimated from Shear-PunchTests

Zone of HAZ of 2.25Cr-1Mo Steel Weldments	Shear Punch Test Results τ_y MPa	τ_u MPa		RA %	Estimated Tensile Property (from correlation equations) YS MPa	UTS MPa	ε_u%	RA %
Inter critical region	310	444	0.093	76	375	539.12	12.83	76.98
Fine-grained bainite	422	520	0.061	52	574.14	690.2	8.153	52.676
Coarse-grained bainite	444	540	0.058	66.6	613.4	730	7.72	67.465

mens extracted from individual microstructures of the HAZ of the 2.25Cr-1Mo weldments and the corresponding uniaxial tensile properties estimated using the correlation established as per Equations 3A, 3B, 9, and 11. The yield strength and ultimate tensile strength values of the 2.25Cr-1Mo weldments (comprising base metal, weld, and HAZ) determined through shear punch tests were found to be in the following order: coarse-grained bainite (CGB), weld metal, fine-grained bainite (FGB), base metal, and intercritical structure (ICR) — Fig. 14. This is in agreement with the earlier results, relating the evolution of microstructures and tensile deformation characteristics of 2.25Cr-1Mo weldments, reported in the literature (Ref. 14). The higher strength of the coarse-grained bainite (CGB) may be attributed to its fine bainitic structure and finer distribution of carbides, while the lower strength of the intercritical structure (ICR) is attributed to the absence of Mo_2C and the reduced bainitic content in this region.

Most of the failure in a 2.25Cr-1Mo weldment is reported to occur in the ICR region. The lower strength of the ICR is consistent with the results of the uniaxial tensile test of a welded joint in which failure in the weld HAZ occurred in the ICR (Ref. 14). It is also found intercritical structure has maximum ductility (% true uniform elongation), while the coarse-grained bainite showed the least. It is clearly seen from Fig. 14 that the fine-grained bainite displayed moderately high strength and adequate ductility while coarse-grained bainite (FGB) had high strength and low ductility and the intercritical zone had minimum strength. The results revealed that neither coarse-grained bainite nor the intercritical structure is a desirable microstructural feature in the HAZ of a weldment. Therefore, it is beneficial to maximize the proportion of fine-grained bainitic microstructure in the HAZ.

The strength values of the three simulated microstructures of 2.25Cr-1Mo, namely the CGB, FGB, and ICR obtained in the present study, have been compared with the strength values of the respective regions of the HAZ in an actual 2.25Cr-1Mo weldment by ShP test methodology. It is seen that differences of about 12% (maximum) in the strength values between the two approaches exist. This may be attributed to the following:

The precipitation kinetics occurring during fast thermal cycles in actual welding could be different from that during simulation. The effects of thermal cycles experienced during multipass welding have not been studied in the simulation techniques. The aim of simulating various microstructures including that of CGB, FGB, and ICR was to obtain a tensile-ShP correlation over a range of strengths expected in an actual weldment. Hence, the strength values estimated using the ShP technique by extracting small specimens from various regions of HAZ could be considered to be the actual strength values in a typical weldment.

Conclusions

1) Reliable correlation between the shear punch test data and uniaxial tensile property was obtained for a variety of microstructures and mechanical properties of 2.25Cr-1Mo steel. This is indicated by degree of scatter (~9 MPa for UTS correlation and ~11 MPa for YS correlation) and the 95% confidence interval (~ ± 2% of σ_u for UTS and ~ ± 2.5% of σ_y for YS) between the actual tensile data and correlation predicted value. True uniform elongation ε_U is linearly related to n_τ, permitting direct estimates of ε_U from ShP tests.

2) Using these correlations and shear punch test, both the strength and ductility parameters of individual regions of HAZ of an actual 2.25Cr-1Mo weldment were estimated. The fine-grained bainitic structure displayed moderately high strength and adequate ductility, while coarse-grained bainite had high strength and low ductility, and the intercritical zone had minimum strength. Therefore, fine-grained bainitic structure is the most desirable microstructure in a 2.25-1Mo weldment.

3) The trends and quantification of gradients in the HAZ of weldments by shear punch test technique are useful in determining the structural integrity of welds and in improving the welding procedures. In addition to this, such tests could also be applied to assess the service-induced degradation of weldments in an actual structure using scooped out specimens, without damaging the structural integrity of the component.

Acknowledgments

The authors thank Dr. P. Rodriguez, director, Indira Gandhi Centre for Atomic Research, for his keen interest and encouragement in this work. The authors express their deep sense of gratitude to Dr. T. P. S. Gill and Dr. A. K. Bhaduri for many useful discussions. The help of R. Parthasarathy and M. Sekar during the course of work is duly acknowledged.

References

1. Akselsen, O. M., and Rorvik, G. 1990. Tensile properties of heat-affected zones of medium strength low carbon, C-Mn, and 2.25Cr-1Mo steels. *Materials Science and Technology* 6: 383–389.

2. Roy, P., and Lauritzen, T. 1986. The relative strengths of base metal and heat-affected zones in 2.25Cr-1Mo weldments — a microstructural evaluation. *Welding Journal* 65(2): 45-s.

3. Lucas, G. E. 1983. Development of small specimen mechanical test techniques. *Journal of Nuclear Materials* 117: 327.

4. Haggag, F. M., Server, W. L., Lucas, G. E., Odette, G. R., and Seckherd, J. W. 1990. The use of miniaturized tests to predict flow properties and estimate fracture toughness in deformed steel plates. *Journal of Testing and Evaluation* 18(1): 62–69.

5. Lucas, G. E. 1990. Review of small specimen test techniques for irradiation testing. *Metallurgical Transactions A*. 214: 1105.

6. Lucas, G. E., Odette, G. R., and Sheckherd, J. W. 1988. Shear punch and microhardness tests for strength and ductility measurements. *The Use of Small-Scale Specimens for Testing Irradiated Materials.* ASTM STP 888. Eds. W. R. Corwin and G. E. Lucas, American Society for Testing and Materials, pp. 112–140.

7. Hamilton, M. L., Toloczko, M. B., and Lucas, G. E. 1995. Recent progress in shear punch testing. *Miniaturized Specimens for Testing of Irradiated Materials.* Eds. H. Ullmaier and P. Jung, pp. 46–58.

8. Hankin, G. L., Johnson, K. I., Khaleel, M. H., Toloczko, M. B., Hamilton, M. L., Davies, R. W., and Faulkner, R. G. 1999. An investigation into the origin and nature of the slope and X-axis intercept of the shear punch-tensile yield strength correlation using finite element analysis. *Effects of Radiation on Materials.* ASTM STP 1366. Eds. M. L. Hamilton, A. S. Kumar, S. T. Rosinski, and M. L. Grossbeck. American Society for Testing and Materials.

9. Wadley, H. N. G., Scruby, C. B., and Spak, H. 1987. Acoustic emission for physical examination of metals. *International Metals Review* 25: 41.

10. Wadley, H. N. G., Scruby, C. B., Lane, P., and Hudson, J. A. 1981. Influence of microstructure on acoustic emission during deformation and fracture of Fe-3.5Ni-0.21C steel. *Metal Science* 15: 514.

11. Kasiviswanathan, K. V., Hotta, S. K., Mukhopadhyay, C. K., and Raj, B. 1998. Miniature shear punch test with on-line acoustic emission monitoring for assessment of mechanical properties. *Small Specimen Test Techniques*. ASTM STP 1329. Eds. W. R. Corwin, S. T. Rosinski, and E. Walle. American Society for Testing and Materials, pp. 523–538

12. Hankin, G. L., Toloczko, M. B., Hamilton, M. L., and Faulkner, R. G. 1998. Validation of the shear punch-tensile correlation technique using irradiated material. *Journal of Nuclear Materials* 258-263: 1651.

13. George, E. Dieter. *Mechanical Metallurgy*, SI Metric Edition. McGraw-Hill Book Co. (U.K.) Ltd., p. 287.

14. Laha, K., Latha, S., Bhanu Sankara Rao, K., and Mannan, S. L. 1993. Temperature dependence of tensile properties of 2.25Cr-1Mo steel base, weldments and simulated heat-affected zone structures, *Transactions of the Indian Institute of Metals* 46(2): 77–87.